HHS Public Access

Author manuscript

Ultrasound Med Biol. Author manuscript; available in PMC 2019 April 24.

Published in final edited form as:

Ultrasound Med Biol. 2018 March ; 44(3): 522–531. doi:10.1016/j.ultrasmedbio.2017.11.018.

AUTOMATED Visualization and Quantification of Spiral Artery Blood Flow Entering the 1st Trimester Placenta using 3D power Doppler Ultrasound.

Gordon N. Stevenson[1], **J. Alison Noble**[2], **Alec W. Welsh**[1,3], **Lawrence Impey**[4], and **Sally L. Collins**[4,5]

[1]School of Womens' & Childrens' Health, Faculty of Medicine, University of New South Wales, Sydney, Australia.

[2]Department of Engineering Science, Institute of Biomedical Engineering, University of Oxford, United Kingdom.

[3]Department of Maternal-Fetal Medicine, Royal Hospital for Women, Randwick, NSW, Australia

[4]The Fetal Medicine Unit, The Women's Centre, John Radcliffe Hospital, Oxford, United Kingdom.

[5]Nuffield Department of Obstetrics and Gynaecology, University of Oxford, Oxford, United Kingdom.

Abstract

To quantify the placental vascularity in 3D at 11–13+6 weeks of pregnancy at precise distances from the utero-placental interface (UPI) using 3D power Doppler (PD) ultrasound. With this automated image analysis technique, differences in vascularity between normal and pathological pregnancies may be observed. The algorithm was validated using a computer-generated image phantom and applied retrospectively in 143 subjects. Scans were conducted with UK (NHS REC) ethical approval. Features from the PD data were recorded, in particular: the number of spiral artery jets into the inter-villous space, total geometric and PD area. These were automatically measured at discrete millimeter distances from the UPI. Differences in features were compared to pregnancy outcomes: pre-eclamptic versus normal, all small-for-gestational (SGA) age to appropriate-for-gestational age (AGA) subjects and AGA versus SGA in normotensives (Mann-Whitney). The Benjamini Hochberg procedure was used (false discovery rate 10%) for multiple comparison testing. Features decreased with increasing distance from the UPI (K-W test; $p < 0.001$). At 2 to 3mm from the UPI, all features were smaller in pre-eclamptic compared to normal subjects and for some in SGA compared to AGA subjects ($p < 0.05$). For AGA versus SGA in normotensive subjects, no significant differences were found. Number of jets measured at 2 to 5mm from the UPI did not vary due to the position of the placenta in the uterus (ANOVA; $p > 0.05$). This method provides a new in-vivo imaging tool for examining spiral artery development through pregnancy. Size and number of entrances of blood-flow into the UPI could potentially be used to identify high-risk pregnancies and may provide a new imaging biomarker for placental insufficiency.

Corresponding Author: Gordon N. Stevenson, Perinatal Imaging Research Group, School of Womens' & Childrens' Health, UNSW, Royal Hospital For Women, Barker Street, Sydney, AU. gordon.n.stevenson@gmail.com Tel +61 (2) 93825272.

Keywords

Diagnostic ultrasound; Infant; small for gestational age; Doppler ultrasound; pre-eclampsia; placenta; Computer-Assisted Image Analysis

Introduction

In pregnancy, trophoblast cells from the developing placenta invade the muscular, tightly coiled walls of the uterine spiral arteries converting them into wide, flaccid conduits. This facilitates the dramatic increase in blood flow required to accommodate the demands of the feto-placental unit. (Pijnenborg, et al. 2006) Impaired transformation of these vessels is widely regarded as the pathology responsible, at least in part, for adverse pregnancy outcomes including pre-eclampsia, utero-placental insufficiency and placental abruption. (Lyall, et al. 2013) Initially, understanding of the pathology was based on histological examination of rare collections of uteri with the placenta still *in-situ* at different gestations. (Burton, et al. 1999) However, the effect on the blood flow through the spiral arteries when trophoblast invasion is reduced cannot be determined from static histological slides and therefore remained almost completely unknown. The pathology may result in a reduced number of spiral arteries which have sufficiently transformed to feed the inter-villous space (IVS), changes in the distribution of the spiral artery jets or reduction in the diameter of their openings resulting in altered haemodynamics within the IVS. With the introduction of ultrasound in pregnancy it was hoped that these questions would be readily answered *in-utero*. Early 2D ultrasound (US) studies however, yielded conflicting results. (Jurkovic, et al. 1991, Murakoshi, et al. 1996) With improvement in Doppler US technology blood flow can now be measured in the IVS from 8 weeks of gestation. (Jauniaux, et al. 2003, Valentin, et al. 1996) The size and velocity waveform of single spiral arteries entering into the IVS have been reproducibly measured by color and pulse-wave Doppler US respectively and demonstrate differences in pathological pregnancies compared to normal ones. (Collins, et al. 2012) Examining single vessels however, cannot fully explain the changes occurring throughout the whole placental bed. A natural extension therefore, is the use of 3D US to simultaneously investigate the whole vascular supply to the placenta. Power Doppler (PD) ultrasound is ideally placed to perform this as it is relatively angle independent, does not alias and is able to measure much slower moving blood flow compared to color Doppler. (Rubin, et al. 1994) Using a combination of 3D and power Doppler (PD) US, the vascularity of the whole utero-placental interface can be examined.

Studies using 3D PD US have attempted to measure the vascularity of the whole placenta but provide conflicting results. This is partly due to the incorporation of the cord insertion and chorionic side of the placenta, meaning both circulatory systems were included rather than simply the maternal side, where the pathology is thought to occur (Welsh, et al. 2005) but mainly due to lack of standardization in the tools available. (Welsh, et al. 2012) These methods also have a degree of operator dependency leading to low reproducibility (Lai, et al. 2010) and require appropriate machine settings which are not always used. (Collins, et al. 2012) These issues aside, the available methods only provide a numerical estimate of overall vascularity. They cannot be used to count the number of individual jets entering the IVS or

to report their size, pattern or distribution. Study of the characteristics of the jets themselves should increase understanding of the development of the placenta in the first trimester. Identifying where differences occur between normal and pathological pregnancies will potentially lead to development of an early screening test to predict women at risk of adverse pregnancy outcomes.

We aimed to develop a medical image analysis based method that can accurately measure image features: the number, size (expressed as cross-sectional area) and distribution of the spiral artery jets entering the IVS. The technique was then validated using a computer-generated 3D vascular phantom and applied to previously collected 3D PD US data. Using this method we aimed to show whether differences in the jets were observed in pregnancies which developed pre-eclampsia and/or resulted in small-for-gestational age (SGA) babies.

Materials and Methods

Computer Generated Phantom

The Insight Toolkit (ITK version 4.8.2; Kitware Inc, Clifton Park, NY, USA) was used to develop a 3D synthetic model (computer-generated phantom) of the placenta. A 3D ellipsoid of radius 128 × 128 × 64 was centered within a 256 × 256 × 128 volume with isotropic spacing of 1mm. The derivative of the image in the direction of short/z axis was then computed to generate normals and the values thresholded at 0 in order to split the ellipsoid into upper or lower hemispheres representative of the maternal or fetal sides of the placenta. Figure 1A shows the surface colored based on the normal calculated on the surface relative to the z-axis. A cut-away view in Fig. 1B shows the signed distance transform generated for the whole 3D ellipsoid showing the distance from the artificial UPI in millimeter increments into the center of the ellipsoid. The signed distance transform provides a labelling of the volume where each voxel is labelled based on the voxel's geometric distance from the UPI signed positive for voxels outside the placenta and negative when within the placenta.

3D jets were then modelled using a 3D Gaussian kernel (11 × 11 × 11 kernel size, $\sigma = 2.0$). The center of the kernel was then placed on the boundary of the maternal side of the ellipsoid (akin to the UPI). Any kernel values set outside of the bounds of the ellipsoid were removed to provide a 3D jet-like pattern within the volume. Phantoms were generated procedurally with different numbers of jets on the UPI surface. 10 computer-generated phantoms were created for each number of jets (10, 20, 30 and 40). Figure 1C shows an example of a 40 jet computer-generated phantom visualized at set distances from 0mm to 3mm of depth from the UPI. With these data constructed, the number of artificial jets and their area were then measured at discrete distances at the UPI in 1mm steps into the model up to 5mm deep reflecting how the entrances of blood into the IVS would be investigated *in-vivo*.

3D PD Ultrasound Acquisition

This work was a retrospective study of scans obtained as part of a prospective study investigating placental imaging biomarkers. This human study was approved by a UK National Health Service Research & Ethics Committee (08/H0604/163). All adult

participants provided written informed consent to participate in this study. 143 women with singleton pregnancies undergoing first-trimester scans between December 2008 and December 2010 were invited to participate and informed written consent was obtained before enrolment. Those under the age of 16 years, those with a body mass index > 35 or significant maternal chronic illnesses, including diabetes and treatment with medications associated with fetal growth restriction, such as beta-blockers were not invited to participate in the study. Sociodemographic and obstetric data were collected, including age, parity, family history, and medical and obstetric histories. Gestational age was calculated from the fetal crown-rump length at the time of scanning. Follow-up consisted of collecting delivery data postpartum by reviewing the hospital notes. The customized birth weight centile was calculated using the Grow software package (version 7.5.1, West Midlands Perinatal Institute, Birmingham, UK). SGA was defined as < 10^{th} centile on customized birth-weight charts with appropriate for gestation age (AGA) babies being those ≥10^{th} centile. Pregnancy associated hypertensive disorders were defined according to the International Society for the Study of Hypertension in Pregnancy (ISSHP) guidelines. (Brown, et al. 2001)

Scanning was performed using a GE Voluson® E8 (GE Healthcare, Milwaukee, WI, USA) and a RAB4–8-D 3D/4D curved array abdominal transducer (4–8.5 MHz). After confirmation of viability and identification of placental position the optimal probe position for 3D acquisition of the whole placenta was identified. This was usually a cross-sectional plane close to the center of the placenta. A 3D PD volume was acquired using the machine settings and quality assurance testing which is fully described in Collins, et al 2012. (Collins 2012)The PD gain in particular was set using the ‘sub-noise gain’ technique which has been previously shown to maximize the PD information available in a 3D acquisition. (Collins, et al. 2012) This is of particular importance when position of the placenta varies by depth depending on implantation on the uterine wall (e.g. anterior, posterior, lateral). With each placental volume captured, the 3D data and specifically the PD signal within the placenta was then analyzed as described.

Visualization and Analysis of Spiral Artery Jets

Scan data was converted offline from polar-coordinate geometry in which ultrasound volumes are typically stored into a 3D Cartesian geometry using a co-ordinate transform and tri-linear interpolation to allow further image analysis. The volumes were processed and resampled using the Visualization and Insight toolkits (Kitware Inc., Clifton Park, NY, USA) as described previously to provide a B-mode and PD volume. (Stevenson, et al. 2015) The algorithm described was coded using C++ and the source code is available online. (https://github.com/gordon-n-stevenson/JetCounting) Figure 2 describes the overall imaging workflow that describes the process to visualize and detect the 3D spiral artery jets of which the conversion result is shown in Fig. 2A.

A segmentation of the placenta was performed using the Random Walker algorithm the formulation of which and application in segmenting the placenta has been described previously (Fig. 2B). (Stevenson, et al. 2015) The segmentation requires a user-initialized seeding to operate which takes between 5–10 minutes to produce and around 40 seconds to compute. (Stevenson, et al. 2015) The segmentation of the placenta provided the

identification of its boundary and so a distance transform was applied to identify voxels within the placenta at discrete distances from the utero-placental interface (UPI) (Fig. 2C). Previous 2D studies of jet length (Collins, et al. 2012) have shown a mean length of 2.76mm (σ = 1.21, range 0.9–7.3). We chose to examine from 2mm away from the UPI to avoid the influence of any artefactual signal from the plexus of vessels in the decidua. An end distance of 5mm was selected as it approximated 2σ away from the mean length of 2D jets measured in the previous studies so we hypothesized this would be an appropriate maximum distance to adequately capture any signal.

The orientation of the surface normal was used to divide the 3D surface within the placenta into the fetal and maternal sides (Fig. 2D). This was performed by re-orientation of the placenta around its centroid with respect to the smallest principal axis (which in an ellipsoidal placenta we assume would represent the axis that best divided the fetal and maternal sides of the placenta). This was performed by principal components analysis, using the Hotelling transform and an affine transformation of the volume.

With the segmentation provided the same geometry as the 3D B-Mode volume, a binary volume, B, was used as where within the volume each voxel was labelled 1 if placenta or otherwise valued 0. The center of mass/centroid of the placenta was calculated and used as the center of rotation around which each volume was transformed. The covariance matrix of B was computed and the axis with the smallest eigenvector used to as the minor axis of the placenta that best separated the fetal and maternal sides of the placenta. With this identified a surface mesh at any choice of distance from the UPI could be computed using the Marching Cubes algorithm. (Lorensen and Cline 1987)

Figure 2D shows a color mapping of the placental surface based on the contribution of the surface normal after affine transformation colored from 1.0 (red; maternal) to −1.0 (blue; fetal). Using a threshold set to zero; the surface was then divided into two and the process repeated for distances 2, 3, 4 and 5mm away from the UPI (Fig. 2E). Determination of which side of the 3D mesh was fetal or maternal was performed by the mass of the PD signal on the boundary of the volume where the large amount of PD signal was considered to be the maternal side as it was inherently more vascular than the fetal side. The output mesh was colored using the scalar information from the PD image volume based on interpolation of the volume data onto the mesh (Fig. 2F). With each vertex colored by PD intensity, isosurface extraction was used using a threshold (96 arb. units) to then extract the individual, distinct areas on the mesh where PD data was found. A video showing the finalized mesh generated with 3D PD data is shown as Movie 1. The following attributes were measured for each mesh and stored to disk for statistical analysis: the total area of the mesh, the area of PD signal, the number of jets. Individual areas < 2mm^2 were considered artefactual and removed from analysis. These attributes were tested for differences between SGA compared to AGA babies in the whole population; SGA compared to AGA in the term, normotensive population and pre-eclamptic pregnancies compared to non pre-eclamptic pregnancies in the whole population.

Statistical Analysis

Statistical analysis was performed using Python and the scipy (version 0.18) and statsmodels (version 0.8) libraries. (Jones, et al. 2001, Seabold and Perktold 2010) Data visualization was performed using Paraview (version 5.1; Kitware Inc, Clifton Park, NY, USA) and graphing using the seaborn plotting library. Normality was determined using the Shapiro-Wilk and Kolmogorov-Smirnoff tests. Differences between outcomes were then tested using the Mann-Whitney or Student's t-test depending on normality. To compensate for multiple comparisons, the Benjamini Hochberg procedure was used with a false discovery rate set at 10%.(Benjamini and Hochberg 1995) Results were considered statistically significant when $p < 0.05$ following correction for multiple comparisons.

Results

Computer-Generated Phantom Study

Table 1 shows the number of jets measured for each computer-generated phantom using the image analysis method at increasing distances from the artificial boundary (UPI). The number of jets measured compared to the actual number generated/positioned upon the computer-generated phantom were then plotted (Fig. 3A) along with mean area (Fig. 3B). Both jet number and area, decreased with increasing distance from the UPI. The results showed that association between estimated jet number and those generated was 100% concordant until 4 to 5mm from the boundary/UPI at which point results deviated. At 5mm, mean number and area were approximately a quarter compared to at the UPI.

Ultrasound Study

143 patients underwent US scanning between 11 weeks 0 days and 13 weeks 6 days' gestation. Mean subject age was 30.5 years ($\sigma = 5.7$; range, 16–44 years), and mean gestational age ± standard deviation at the time of scanning was 90 days ($\sigma = 4.4$; range, 80–97 days). 139 women delivered after 37 weeks' gestation of whom 126 were normotensive (had normal blood pressure readings) throughout pregnancy. Eight subjects developed pre-eclampsia and five pregnancy induced hypertension. Of the four that delivered before 37 weeks, two were appropriate-for-gestational age (AGA) for gestation, one was SGA and one was SGA with pre-eclampsia. Using customized centile charts (Gardosi, et al. 2011), 20 babies were SGA. There were no significant differences in baseline demographics for any of the groups. (Collins, et al. 2013)

All subjects had successful measurement 2mm from the UPI but at 3mm, 1 patient was not able to be analyzed (0.7%) and at 4 and 5mm this increased to 3 patients (2.1%). These patients were excluded as the placentas were so thin that the fetal blood supply was close enough to potentially be measured automatically by the method thereby contaminating the results. Due to the poor approximation of the number and size of jets at 5mm in the computer-generated phantom study, a decision was made to discard measurements made at this distance and consider only those at 2 to 4 mm from the UPI.

Number of jets, mean geometric area of the placenta at a set distance from the UPI and area of PD signal measured at the same distance from the UPI were calculated at millimeter

increments from 2mm to 4mm. All features decreased in value with increasing distance from the UPI (K-W test; $p < 0.001$). Figure 4 shows a rendering of four meshes taken from a single subject indicating the reduction of the PD signal as distance increases from the UPI. The figure illustrates that, where PD signal is present and of a sufficiently strong response at 2mm from the UPI, subsequent meshes deeper into the placenta contain PD signals at similar positions. The jet number and total area of these regions of PD signal diminishes as shown at 3 and 4mm. The clustering of particular areas of PD signal appears to be consistent between different levels, indicating that this 3D technique is able to both capture 2D entrances of blood in a cross-sectional manner and show their progression into the IVS.

Position of the placenta was recorded by operator at the time of the scan and comparison between the number of jets was analyzed for those who were AGA at term. The placental position was recorded as: 49 anterior, 48 posterior, 14 lateral, 9 fundal and 2 previa. The previa cases were excluded from analysis and one-way analysis of variance (ANOVA) was performed. Figure 5 shows the number of jets per placental position at different distances from the UPI. No significant differences ($p > 0.05$) were observed when comparing number of jets at these distances against placental location.

Table 2 shows the results between all SGA subjects against AGA. Significant differences were found ($p < 0.05$) for both the number and area of PD signal present as well as total geometric area at 2mm and 3mm away from the UPI. At 4mm, only number of jets was significantly different ($p = 0.037$). When comparing the normotensive SGA group with normotensive AGA, no significance differences were found in any features (Table 3). In the pre-eclamptic group compared to normal, significant differences ($p > 0.05$) for all features at all distances from the UPI were observed (Table 4).

Discussion

This work represents, to the best of our knowledge, the first attempt to automatically count and measure the jets of blood flowing into the IVS of an entire placenta *in-utero*. Study of this vascular system is fundamental to increasing our understanding of the pathology underlying many conditions resulting in adverse pregnancy outcome including pre-eclampsia and fetal growth restriction. Current understanding of placental circulation is that blood from the maternal vasculature enters the IVS as a jet from the terminal end of the spiral arteries, gradually slowing in velocity as it circulates around the IVS before draining back through multiple small venous sinuses. Figure 4 shows that cross-sectional slices through these jets can be made at set distances from the UPI as they progress into the IVS. The radii of these jets decreased as they pass deeper into the IVS. This is most likely to represent a decreasing amount of blood flowing at a sufficiently high velocity that it can be recorded with PD US reinforcing observations made using 2D US. (Collins, et al. 2012) By application of a signed distance transform (Maurer Jr, et al. 2003) on the data we are able to isolate, with confidence, voxels which should only contain maternal blood. As the transform is applied on a whole placenta which is subdivided into maternal and fetal sides, all voxels that are closer to the fetal side of the organ are automatically removed. This is of particular importance in the placenta as there are haematological differences between the maternal and fetal blood systems which may alter the appearance of PD. (Welsh, et al. 2005)

It is not only differences in the size and number of spiral arteries that has been implicated in placental pathology but their distribution (peripheral vs central location) may be altered in abnormal pregnancies. Attempts have been made to examine this using 2D US however, some researchers have doubted the ability of US to assess the extent of spiral artery remodeling in the lateral aspects of the placenta. (Brosens, et al. 2011) We believe that our imaging method can solve this problem and represents a step towards identifying the pattern of vascular remodeling seen in the placenta *in-utero*. By capturing the whole organ in 3D, both central and peripheral vasculature is acquired completely (as shown in Figure 2) without the need for multiple 2D scans and transducer movement. The lateral extent of modelling can then be compared to the central and overall vascularization visualized. Automatic reporting and subsequent analysis of the position and distribution of the spiral arteries is therefore a natural extension of this work.

A 3D synthetic model showed the trends in decrease in jet size and number that we would expect when in-utero scanning. Based on this preliminary work and with the image processing technique developed we successfully observed that 3D PD features (the number of jets, total surface area and total PD area) were significantly lower in the first-trimester placenta that resulted in a pre-eclamptic pregnancy. These differences were not found for the term, normotensive SGA pregnancies indicating that these pregnancies have similar vascularity to pregnancies destined to produce normally grown babies. With further work it is conceivable that this technique could potentially provide automated imaging biomarkers that might aid the early prediction of adverse pregnancy outcomes.

We acknowledge that this work does have limitations. A physical tissue-mimicking flow phantom or animal model has not been used to validate to our method. However, since PD can show excellent reconstructions of the utero-placenta vasculature in 3D (*28*) (see supplementary Movie 1) and vascular changes in 2D PD have shown to correlate with changes in perfusion (Hernandez-Andrade, et al. 2004, Rubin, et al. 1997), we feel it was appropriate to proceed with *in-utero* investigations and have confidence that 3D PD measurements reflect actual vascularity. A potential difficulty of volumetric measurement is the subjectivity of organ segmentation. This was mitigated by using a segmentation method that has been validated in a repeatability study and shown to provide good levels of reproducibility both within and between observers. (Stevenson, et al. 2015) It is hoped in future work that the application of a fully automatic deep learning segmentation method that requires no user initialization will be used to reduce this source of potential error. (Looney, et al. 2017) An analysis of how reproduciblse visualization results are based on different segmentations of the placenta as well as the impact of machine settings and different ultrasound systems should be a priority for future work.

The number, size and distribution of spiral arteries in the average placenta is yet to be definitively demonstrated. Estimates from histological specimens examined at > 37 weeks gestation varies from 30 to 120. (Brosens and Dixon 1966, Reynolds 1966) We were able to visualize considerably less in the first trimester. Whether we are only demonstrating spiral arteries with sufficient blood flow to be detected using 3D PD imaging or these PD signals represent a conglomeration of flow from the distal ends of multiple spiral arteries remains unknown; understanding this would require longitudinal data which was not available. We

hope that by further study using this method a comparison between features as measured by 3D PD US can be compared to pathological specimens.

The image processing method described has shown that it can successfully display and quantify total area and quantity the specific areas of PD signal representing entry of arterial blood into the IVS in a study of 143 pregnancies. Following initial segmentation of the placenta, the method is fully automated and has the potential to rapidly assess the magnitude and distribution of blood flow within the placenta in early pregnancy in 3D for the first time. In the case of the placenta, this could provide a method to complement previous histological studies of spiral arteries and investigate changes in vascularity throughout pregnancy. With this method available as open-source software, combined with the move toward open availability of 3D US data in a common, vendor agnostic format (Freesmeyer, et al. 2012) it is hoped that larger cohorts of data across multiple centers can be collected for further study. With large-scale data the ability of these 3D PD US features to detect early indications of various obstetrical pathology may be determined. These automated tools could then be used to assess placental vascular changes through pregnancy and hopefully identify US biomarkers for adverse pregnancy outcomes as early as the first trimester.

Supplementary Material

Refer to Web version on PubMed Central for supplementary material.

Acknowledgements

We thank the staff of the ultrasound department at the Women's Centre, John Radcliffe Hospital, especially Ms. Katie Blissett, for all their help recruiting the study participants. Research reported in this publication was supported by the Eunice Kennedy Shriver National Institute of Child Health and Human Development (NICHD) Human Placenta Project of the National Institutes of Health under award number UO1HD087209. The content is solely the responsibility of the authors and does not necessarily represent the official views of the National Institutes of Health. The Oxford Partnership Comprehensive Biomedical Research Centre supported G.N.S and S.L.C with funding from the Department of Health National Institute of Health Research (NIHR) Biomedical Research Centre's funding scheme. G.N.S is supported by a philanthropic grant from the Leslie Stevens Fund for Newborn Care, Sydney.

References

Benjamini Y, Hochberg Y. Controlling the false discovery rate: a practical and powerful approach to multiple testing. Journal of the royal statistical society. Series B (Methodological) 1995:289–300.

Brosens I, Dixon HG. The Anatomy of the Maternal Side of the Placenta. BJOG: An International Journal of Obstetrics & Gynaecology 1966; 73:357–63.

Brosens I, Pijnenborg R, Vercruysse L, Romero R. The "Great Obstetrical Syndromes" are associated with disorders of deep placentation. American Journal of Obstetrics and Gynecology 2011; 204:193–201. [PubMed: 21094932]

Brown MA, Lindheimer MD, de Swiet M, Assche AV, Moutquin J-M. The classification and diagnosis of the hypertensive disorders of pregnancy: statement from the International Society for the Study of Hypertension in Pregnancy (ISSHP). Hypertension in pregnancy 2001; 20:ix–xiv. [PubMed: 12044323]

Burton GJ, Jauniaux E, Watson AL. Maternal arterial connections to the placental intervillous space during the first trimester of human pregnancy: The Boyd Collection revisited. American Journal of Obstetrics & Gynecology 1999; 181:718. [PubMed: 10486489]

Collins S 2012 Development of placental ultrasound markers to screen for the term, small for gestational age (SGA) baby: University of Oxford.

Collins S, Stevenson G, Noble J, Impey L, Welsh A. Influence of power Doppler gain setting on Virtual Organ Computer-aided AnaLysis indices in vivo: can use of the individual sub-noise gain level optimize information? Ultrasound in Obstetrics & Gynecology 2012; 40:75–80. [PubMed: 22009687]

Collins SL, Birks JS, Stevenson G, Papageorghiou A, Noble J, Impey L. Measurement of the spiral artery jets: general principles and differences observed for small for gestational age (SGA) babies. Ultrasound in Obstetrics & Gynecology 2012; 40:171–78. [PubMed: 22102536]

Collins SL, Stevenson GN, Noble JA, Impey L. Rapid Calculation of Standardized Placental Volume at 11 to 13 Weeks and the Prediction of Small for Gestational Age Babies. Ultrasound in Medicine & Biology 2013; 39:253–60. [PubMed: 23219036]

Freesmeyer M, Darr A, Schierz J-H, Schleußner E, Wiegand S, Opfermann T. 3D ultrasound DICOM data of the thyroid gland: First experiences in exporting, archiving, second reading and 3D processing. Nuklearmedizin 2012; 51:73–78. [PubMed: 22526598]

Gardosi J, Figueras F, Clausson B, Francis A. The customised growth potential: an international research tool to study the epidemiology of fetal growth. Paediatric and Perinatal Epidemiology 2011; 25:2–10. [PubMed: 21133964]

Hernandez-Andrade E, Jansson T, Ley D, Bellander M, Persson M, Lingman G, Marsàl K. Validation of fractional moving blood volume measurement with power Doppler ultrasound in an experimental sheep model. Ultrasound in Obstetrics and Gynecology 2004; 23:363–68. [PubMed: 15065186]

Jauniaux E, Hempstock J, Greenwold N, Burton GJ. Trophoblastic oxidative stress in relation to temporal and regional differences in maternal placental blood flow in normal and abnormal early pregnancies. The American Journal of Pathology 2003; 162:115–25. [PubMed: 12507895]

Jones E, Oliphant T, Peterson P, others. SciPy: Open source scientific tools for Python, 2001.

Jurkovic D, Jauniaux E, Kurjak A, Hustin J, Campbell S, Nicolaides KH. Transvaginal color Doppler assessment of the uteroplacental circulation in early pregnancy. Obstetrics & Gynecology 1991; 77:365. [PubMed: 1992400]

Lai PK, Wang YA, Welsh AW. Reproducibility of regional placental vascularity/perfusion measurement using 3D power Doppler. Ultrasound in Obstetrics and Gynecology 2010; 36:202–09. [PubMed: 20201118]

Looney P, Stevenson GN, Nicolaides KH, Plasencia W, Molloholli M, Natsis S, Collins SL. 2017 Automatic 3D Ultrasound Segmentation of the First Trimester Placenta using Deep Learning. IEEE International Symposium on Biomedical Imaging. Melbourne: IEEE.

Lorensen WE, Cline HE. 1987 Marching cubes: A high resolution 3D surface construction algorithm. ACM siggraph computer graphics: ACM, 163–69.

Lyall F, Robson SC, Bulmer JN. Spiral artery remodeling and trophoblast invasion in preeclampsia and fetal growth restriction: relationship to clinical outcome. Hypertension 2013; 62:1046–54. [PubMed: 24060885]

Maurer CR Jr, Qi R, Raghavan V. A linear time algorithm for computing exact euclidean distance transforms of binary images in arbitrary dimensions. Pattern Analysis and Machine Intelligence, IEEE Transactions on 2003; 25:265–70.

Murakoshi T, Sekizuka N, Takakuwa K, Yoshizawa H, Tanaka K. Uterine and spiral artery flow velocity waveforms in pregnancy-induced hypertension and/or intrauterine growth retardation. Ultrasound in Obstetrics & Gynecology 1996; 7:122–28. [PubMed: 8776237]

Pijnenborg R, Vercruysse L, Hanssens M. The Uterine Spiral Arteries In Human Pregnancy: Facts and Controversies. Placenta 2006; 27:939–58. [PubMed: 16490251]

Reynolds SR. Formation of fetal cotyledons in the hemochorial placenta. A theoretical consideration of the functional implications of such an arrangement. American Journal of Obstetrics and Gynecology 1966; 94:425–39. [PubMed: 5324149]

Rubin J, Bude R, Fowlkes J, Spratt R, Carson P, Adler R. Normalizing fractional moving blood volume estimates with power Doppler US: defining a stable intravascular point with the cumulative power distribution function. Radiology 1997; 205:757. [PubMed: 9393532]

Rubin JM, Bude RO, Carson PL, Bree RL, Adler RS. Power Doppler US: a potentially useful alternative to mean frequency-based color Doppler US. Radiology 1994; 190:853. [PubMed: 8115639]

Seabold S, Perktold J. Statsmodels: Econometric and statistical modeling with python. Proceedings of the 9th Python in Science Conference 2010:57–61.

Stevenson GN, Collins SL, Ding J, Impey L, Noble JA. 3-D Ultrasound Segmentation of the Placenta Using the Random Walker Algorithm: Reliability and Agreement. Ultrasound in Medicine & Biology 2015; 41:3182–93. [PubMed: 26341043]

Stevenson GN, Collins SL, Welsh AW, Impey LW, Noble JA. A Technique for the Estimation of Fractional Moving Blood Volume by Using Three-dimensional Power Doppler US. Radiology 2015; 274:230–37. [PubMed: 25117590]

Valentin L, Sladkevicius P, Laurini R, Söderberg H, Marsal K. Uteroplacental and luteal circulation in normal first-trimester pregnancies: Doppler ultrasonographic and morphologic study. American journal of obstetrics and gynecology 1996; 174:768–75. [PubMed: 8623819]

Welsh A, Collins S, Stevenson G, Noble J, Impey L. Inapplicability of the Fractional Moving Blood Volume (FMBV) technique to standardise VOCAL indices for quantified power Doppler. Ultrasound in Obstetrics & Gynecology 2012.

Welsh A, Rubin J, Fowlkes J, Fisk N. Standardization of power Doppler quantification of blood flow in the human fetus using the aorta and inferior vena cava. Ultrasound in Obstetrics and Gynecology 2005; 26:33–43. [PubMed: 15971284]

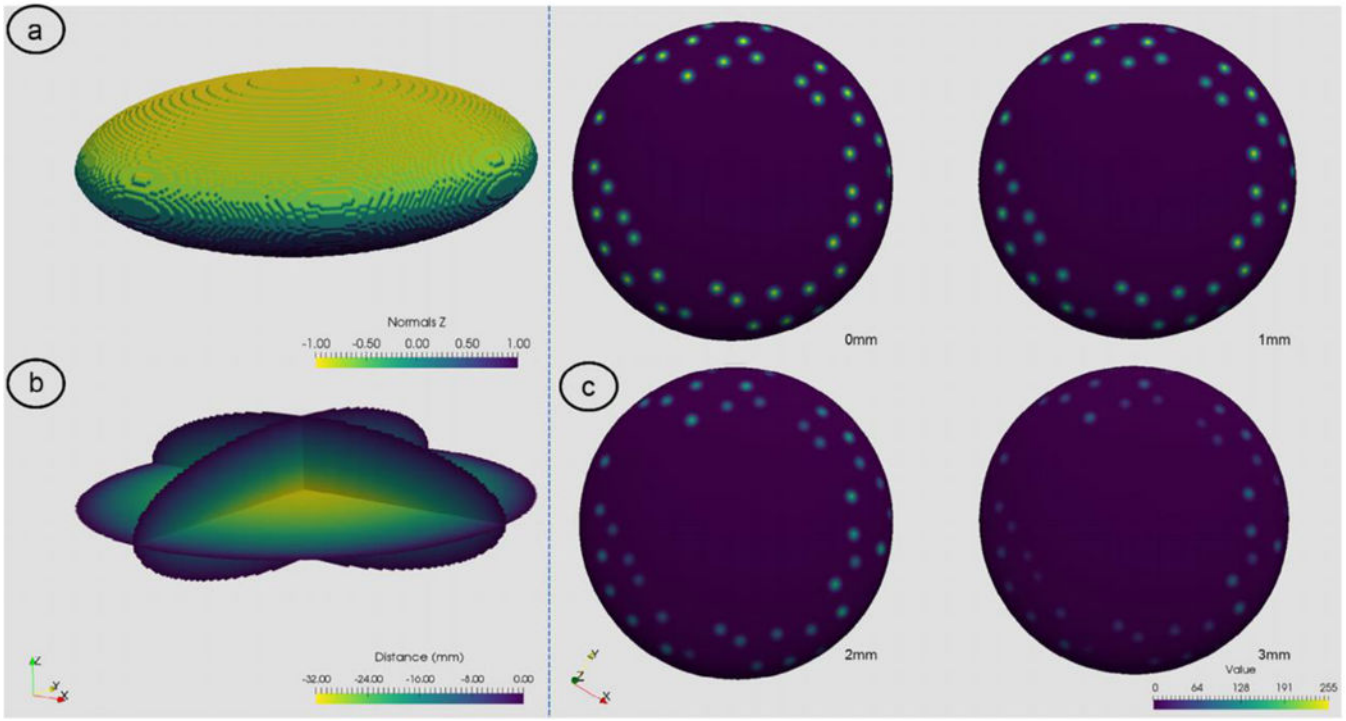

Figure 1.

Visualization of 3D ellipsoid used for measurement validation. (A) shows a 3D contour of the surface of the ellipsoid colored based upon the z values of the surface normals; (B) the signed-distance transform colored by distance from the ellipsoid surface; (C) the UPI surface extracted based on the surface normals values with following the 3D jet data added to the ellipsoid. In this example, 40 jets were randomly placed on the surface and then visualized at 0 to 3mm from the boundary.

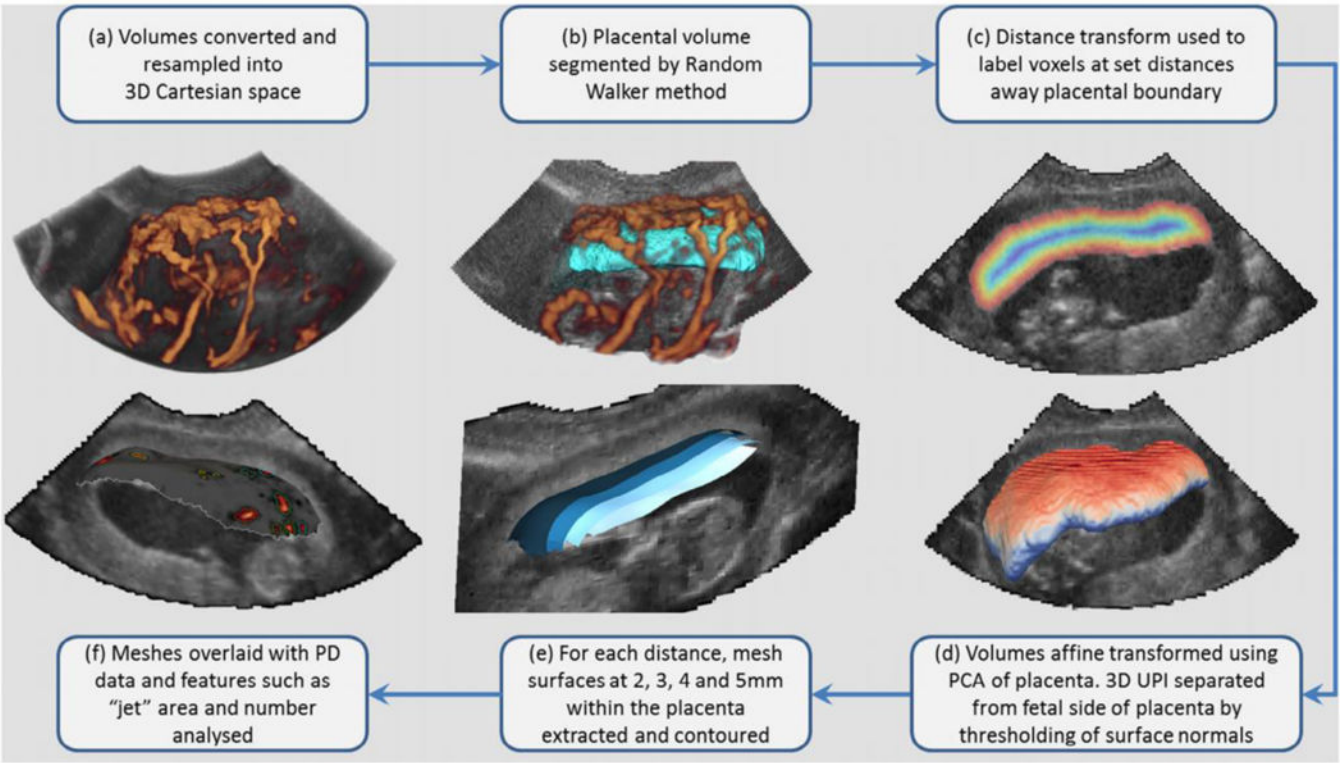

Figure 2.

Workflow of image processing method to generate 3D meshes for analysis of power Doppler (PD) signal at specific distances on the maternal side of the placenta. From clockwise: 3D PD volume rendering following conversion of data showing PD (orange) and B-Mode (greyscale) (A). Placental volume (teal) with PD rendering and 2D B-Mode slice (B). Distance transform (multicolor) based on millimetre distance away from placental boundary (C). 3D placenta volume color mapped based on surface normal of single axis where blue indicates the fetal side and red the maternal (D). 3D surfaces colored from blue to white representing each of the four distances within the placenta analyzed converted from voxel to mesh data (E). Finally, a 2mm mesh is shown with PD data overlaid upon the surface and each closed PD signal above the noise threshold outlined as a specific region of interest (F).

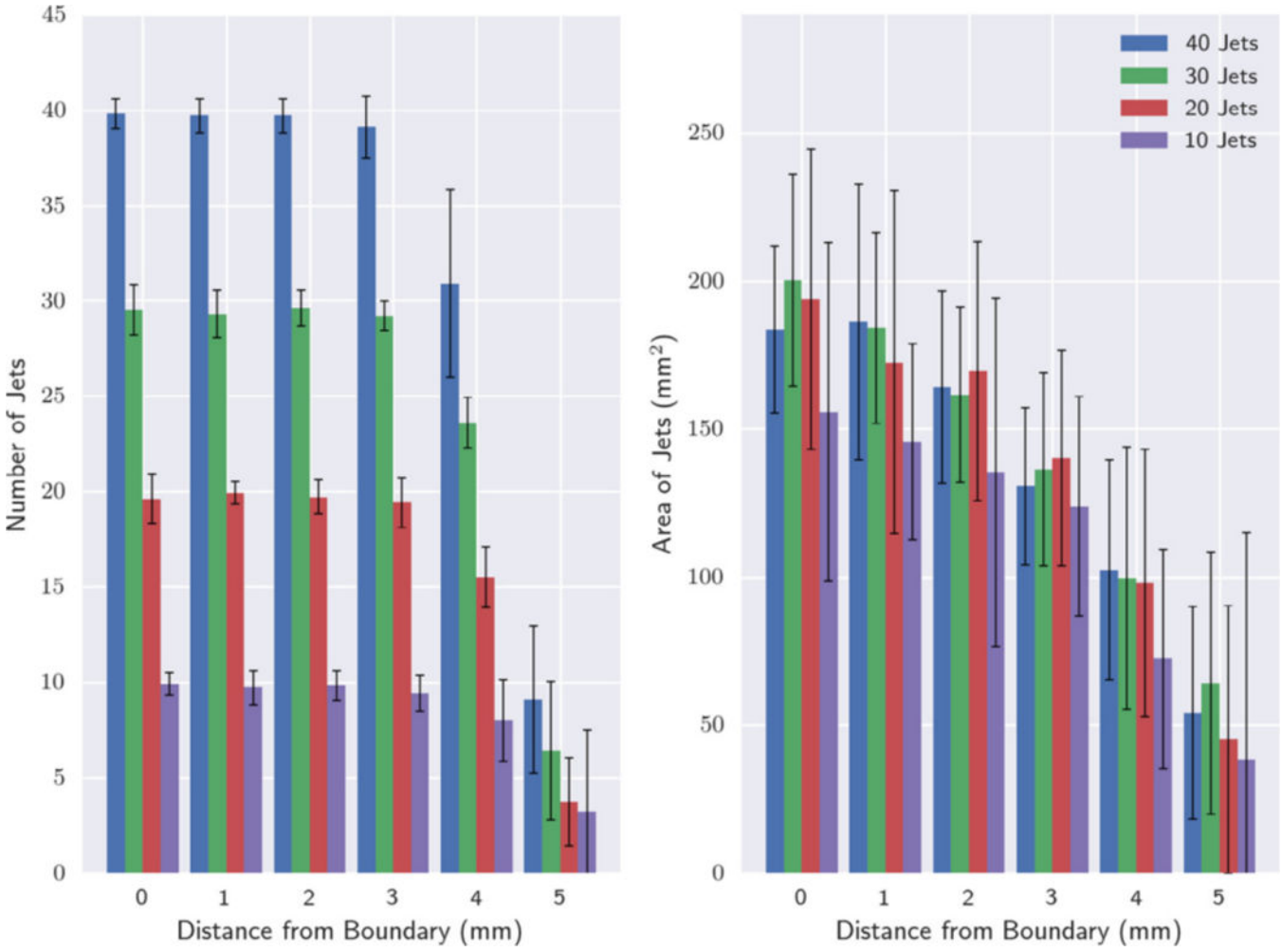

Figure 3.

Graph showing number of jets and mean areas measured in the set of 3D ellipsoid computer-generated phantoms with 10 to 40 generated jets. (A) Number of discrete areas measured at distances 0 to 5mm from the ellipsoidal boundary. (B) Mean area as measured for each identified jet measured at 0 to 5mm from the boundary.

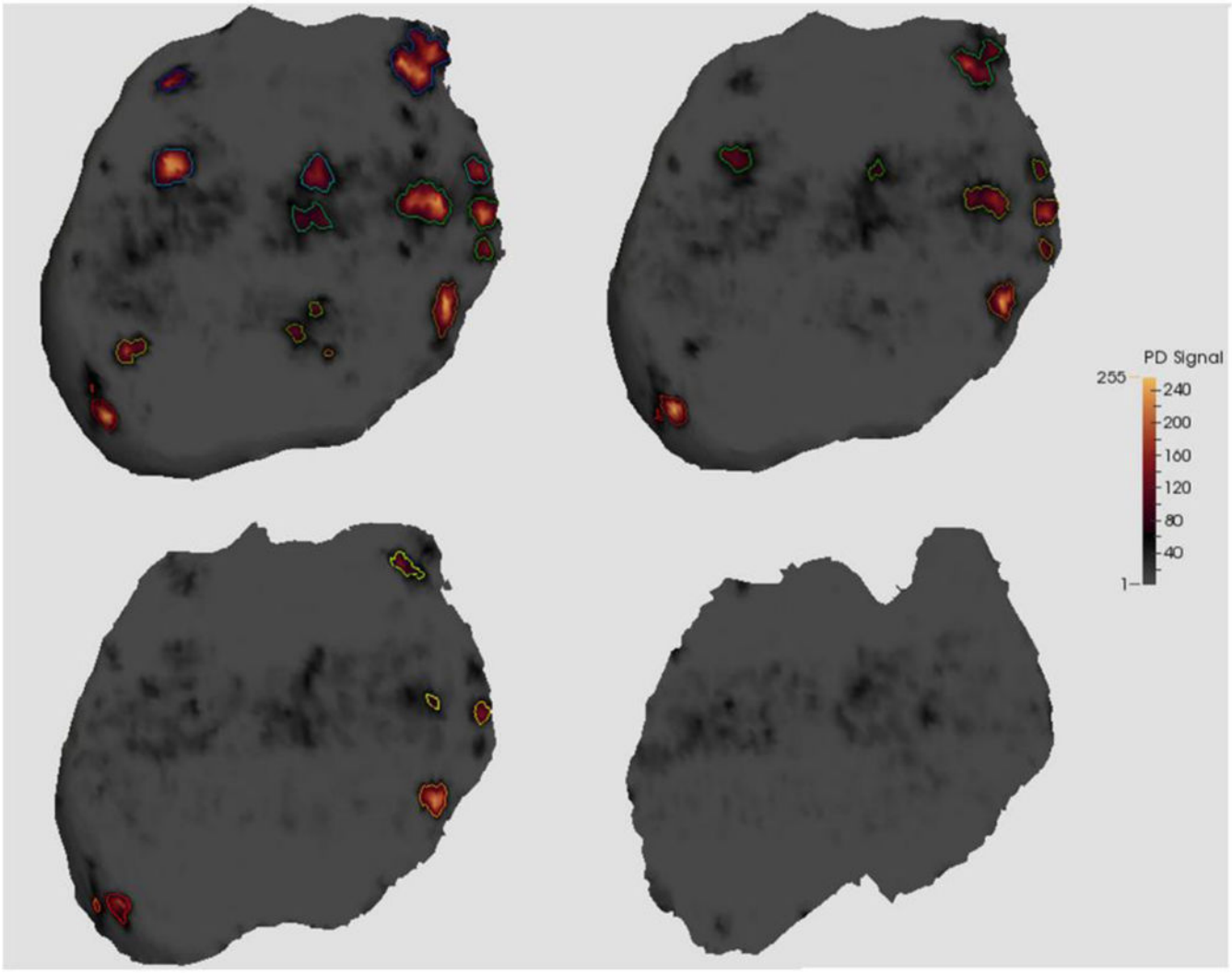

Figure 4.

Example of meshes visualized for a single patient within the placenta at two to five millimeters from the utero-placental interface (UPI). Data is from 2mm (top left), 3mm (top right), 4mm (bottom left) and 5mm (bottom right) the UPI. For each mesh, enclosed PD signal was found and outlined to show each individual “jet” of signal.

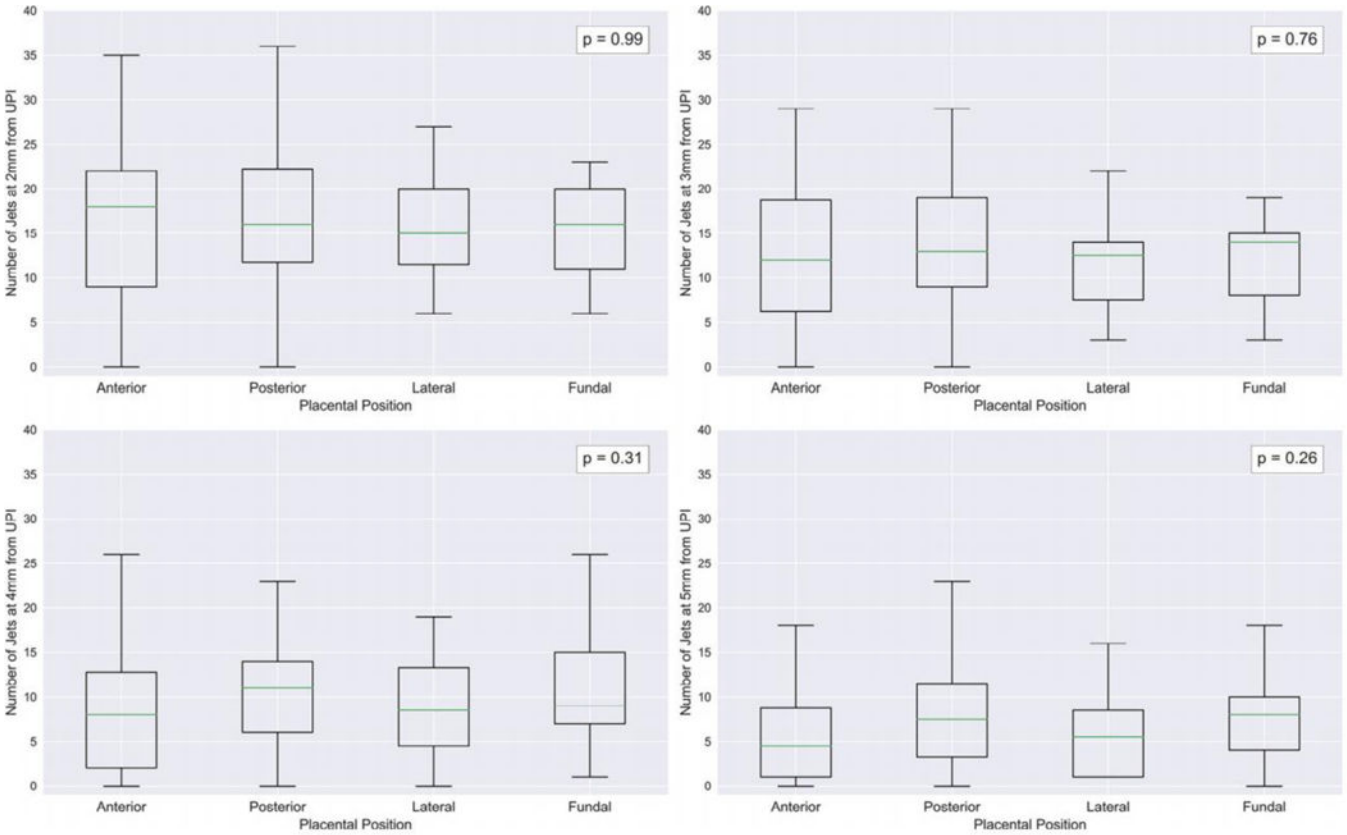

Figure 5.

Boxplot of number of jets measured for each placental position (anterior, posterior, lateral and fundal) for appropriate for gestational age (AGA) subjects measured at 2 to 5mm from the UPI. Legend shows p-values reported at each distance by one-way analysis of variance (ANOVA).

Table 1.

Number of estimated jets and mean area at distances from boundary of computer-generated phantom compared to those generated procedurally for computer-generated phantom.

		Distance From Utero-Placental Interface					
Jet Number	**Measure**	**0mm**	**1mm**	**2mm**	**3mm**	**4mm**	**5mm**
10	Number ($\mu \pm \sigma$)	9.9 ± 0.3	9.7 ± 0.5	9.8 ± 0.4	9.4 ± 0.5	8.0 ± 1.1	3.2 ± 2.2
	Area ($mm^{2;}$ $\mu \pm \sigma$)	155.6 ± 29.2	145.5 ± 16.9	135.3 ± 30	123.8 ± 18.9	72.3 ± 18.9	38.3 ± 39
20	Number ($\mu \pm \sigma$)	19.6 ± 0.7	19.9 ± 0.3	19.7 ± 0.5	19.4 ± 0.7	15.5 ± 0.8	3.7 ± 1.2
	Area ($mm^{2;}$ $\mu \pm \sigma$)	193.8 ± 25.9	172.4 ± 29.5	169.5 ± 22.3	140.1 ± 18.6	97.8 ± 23	44.9 ± 23.1
30	Number ($\mu \pm \sigma$)	29.5 ± 0.7	29.3 ± 0.6	29.6 ± 0.5	29.2 ± 0.4	23.6 ± 0.7	6.4 ± 1.8
	Area ($mm^{2;}$ $\mu \pm \sigma$)	200.2 ± 18.2	184 ± 16.4	161.5 ± 15.2	136.2 ± 16.6	99.5 ± 22.6	64.2 ± 22.6
40	Number ($\mu \pm \sigma$)	39.8 ± 0.4	39.7 ± 0.5	39.7 ± 0.5	39.1 ± 0.8	30.9 ± 2.5	9.1 ± 2.0
	Area ($mm^{2;}$ $\mu \pm \sigma$)	183.5 ± 14.4	186.1 ± 23.7	164.1 ± 16.6	130.6 ± 13.5	102.3 ± 18.9	54 ± 18.3

Table 2.

Summary of jet number, total surface area and total PD area between appropriate-for-gestational age and small-for-gestational age (SGA) subjects.

			AGA		SGA	
Measure	Distance	n	Mean ± Std. Dev	n	Mean ± Std. Dev	p
Number of Jets	2mm	123	17.25 ± 9.40	20	12.30 ± 9.69	0.028
Total Area (cm^2)			52.50 ± 17.36		42.47 ± 13.98	0.032
Total PD Area (cm^2)			7.61 ± 5.39		5.71 ± 6.56	0.052
Number of Jets	3mm	122	13.39 ± 7.61	20	8.45 ± 7.60	0.015
Total Area (cm^2)			47.38 ± 16.56		38.25 ± 13.67	0.035
Total PD Area (cm^2)			5.83 ± 4.77		4.20 ± 5.29	0.042
Number of Jets	4mm	122	9.57 ± 6.25	18	6.56 ± 7.03	0.037
Total Area (cm^2)			41.25 ± 14.76		34.95 ± 11.41	0.08
Total PD Area (cm^2)			3.53 ± 3.29		2.81 ± 3.18	0.188

Table 3.

Summary of jet number, total surface area and total PD area between normotensive appropriate-for-gestational age and normotensive small-for-gestational age (SGA) subjects.

		NORMOTENSIVE AGA		NORMOTENSIVE SGA		
Measure	Distance	n	Mean ± Std. Dev	n	Mean ± Std. Dev	p
Number of Jets	2mm	129	16.65 ± 9.63	14	15.71 ± 9.24	0.328
Total Area (cm^2)			51.46 ± 17.74		47.70 ± 11.49	0.326
Total PD Area (cm^2)			7.32 ± 5.45		7.56 ± 6.96	0.452
Number of Jets	3mm	128	12.88 ± 7.83	14	11.00 ± 7.31	0.258
Total Area (cm^2)			46.39 ± 16.94		43.37 ± 11.15	0.328
Total PD Area (cm^2)			5.62 ± 4.78		5.47 ± 5.73	0.388
Number of Jets	4mm	126	9.36 ± 6.31	14	7.64 ± 7.31	0.189
Total Area (cm^2)			40.78 ± 14.84		37.39 ± 10.92	0.299
Total PD Area (cm^2)			3.46 ± 3.28		3.25 ± 3.31	0.427

Table 4.

Summary of jet number, total surface area and total PD area between normal and pre-eclamptic (PET) subjects.

			NON-PET		PET	
Measure	Distance	n	Mean ± Std. Dev	n	Mean ± Std. Dev	p
Number of Jets	2mm	134	17.23 ± 9.41	9	6.56 ± 5.70	0.005
Total Area (cm^2)			52.23 ± 16.96		34.11 ± 11.99	0.008
Total PD Area (cm^2)			7.69 ± 5.56		2.15 ± 2.76	0.005
Number Oo Jets	3mm	133	13.26 ± 7.61	9	4.22 ± 4.84	0.005
Total Area (cm^2)			47.19 ± 16.19		29.91 ± 11.62	0.008
Total PD Area (cm^2)			5.86 ± 4.89		1.84 ± 2.14	0.01
Number of Jets	4mm	133	9.47 ± 6.38	7	3.71 ± 4.19	0.028
Total Area (cm^2)			41.06 ± 14.50		28.52 ± 8.17	0.032
Total PD Area (cm^2)			3.54 ± 3.30		1.42 ± 1.83	0.045